IOPscience iopscience.iop.org

Home Search Collections Journals About Contact us My IOPscience

Quadrupole effects and electron-phonon interaction in the non-equilibrium superconductors $Al_{1-x}Si_x$

This article has been downloaded from IOPscience. Please scroll down to see the full text article.

2000 J. Phys.: Condens. Matter 12 9167

(http://iopscience.iop.org/0953-8984/12/43/307)

View the table of contents for this issue, or go to the journal homepage for more

Download details:
IP Address: 171.66.16.221
The article was downloaded on 16/05/2010 at 06:56

Please note that terms and conditions apply.

J. Phys.: Condens. Matter **12** (2000) 9167–9178. Printed in the UK PII: S0953-8984(00)14088-3

Quadrupole effects and electron–phonon interaction in the non-equilibrium superconductors $Al_{1-x}Si_x$

A A Gippius†, N E Sluchanko‡¶, V V Glushkov‡, S V Demishev‡, M V Kondrin‡, A A Pronin‡, V V Brazhkin§, V V Moshchalkov‖ and Y Bruynseraede‖

† Faculty of Physics, Moscow State University, 119899, Vorob'evy Gory, Moscow, Russia
‡ General Physics Institute, Russian Academy of Sciences, Vavilova Street 38,117942, Moscow, Russia
§ Institute of High Pressure Physics, Russian Academy of Sciences, 142092, Troitsk, Moscow Region, Russia
‖ Laboratory voor Vaste-Stoffysica en Magnetisme, K U Leuven, Celestijnenlaan 200 D, B-3001 Leuven, Belgium

E-mail: nes@lt.gpi.ru (N E Sluchanko)

Received 22 May 2000, in final form 18 September 2000

Abstract. ^{27}Al NMR (nuclear magnetic resonance) spectra and the spin–lattice relaxation were measured for the non-equilibrium Al-based superconductors $Al_{1-x}Si_x$ ($x = 0$, 0.02, 0.05, 0.06 and 0.08) in the temperature range 2–300 K. The NMR data confirm a substantial enhancement of the electron–phonon interaction in the vicinity of the FCC (face-centred cubic) lattice instability in these model superconductors. The observed quadrupole effects can be interpreted in terms of a substantial distortion and disordering of the Al-based FCC lattice.

1. Introduction

The superconducting transition temperature T_c of bulk metallic Al is about 1.18 K [1]. Thin granulated Al films prepared by deposition on a cold substrate exhibit superconductivity with T_c up to 3.7 K. The increase of T_c for Al may be caused by the exposure of the sample to neutron or ion (H, D, O and others) beams. In some cases the T_c-value approaches 6 K [2], and with ion implantation of C, Si and Ge in Al it reaches $T_c(C) = 4.2$ K, $T_c(Ge) = 7.35$ K, $T_c(Si) = 8.35$ K [3], but the superconducting phase becomes metastable. According to [4], for the Al–B alloys (B = Si, Ge) synthesized by fast quenching from the melt, an enhancement of the superconductivity also takes place and the transition temperature approaches 7.5 K. All of these examples of superconductivity enhancement in Al demonstrate different realizations of disorder of the Al-based crystal structure. In most cases the disorder is accompanied by the appearance of a metastable superconducting phase based on an Al FCC matrix [1–4]. However, the complicated synthesis procedure used in [1–4] and the inhomogeneity of the real samples have prevented a quantitative analysis of the superconducting state parameters within the framework of existing models.

The investigations of the T–X phase diagrams of the Al–Si and Al–Ge systems in [5] revealed a significant elevation of the Si and Ge solubility in Al under high pressure (see

¶ Author to whom any correspondence should be addressed.

0953-8984/00/439167+12$30.00 © 2000 IOP Publishing Ltd

the inset in figure 1). Non-equilibrium FCC solid solutions $Al_{1-x}Si_x$ and $Al_{1-x}Ge_x$ were synthesized [6] under high pressure (up to 10 GPa) in the concentration range $x < 0.2$. In the case of $Al_{0.8}Si_{0.2}$, the superconducting transition temperature T_c was found to rise to 11 K [6] (figure 1(a)). It is worth emphasizing that in order to reach the content range $x > 0.1$, the non-equilibrium solid solutions $Al_{1-x}Si_x$ were synthesized in [6] under high pressure by quenching to liquid-nitrogen temperatures. Due to these technological achievements, the non-equilibrium model superconductors $Al_{1-x}Si_x$ have been obtained, as homogeneous single-phase FCC metallic compounds with T_c-changes of about an order of magnitude (between 1.18 K and 11 K). Moreover, a simple Fermi surface constructed from only s- and p-electronic states together with a simple relation between the Si concentration x and T_c (figure 1(a)) are the main factors which lead one to consider these alloys as a very promising model system for studying the nature of the superconductivity enhancement in the vicinity of the lattice instability in metals. To avoid any adverse effects connected with the phase separation process and second phase formation in these non-equilibrium compounds and to concentrate only on studying the superconducting and normal-state properties of the single-phase $Al_{1-x}Si_x$ solid solutions, a comprehensive investigation of the decay kinetics and of the non-equilibrium state parameters has been carried out recently [7–9]. It was clearly established that these

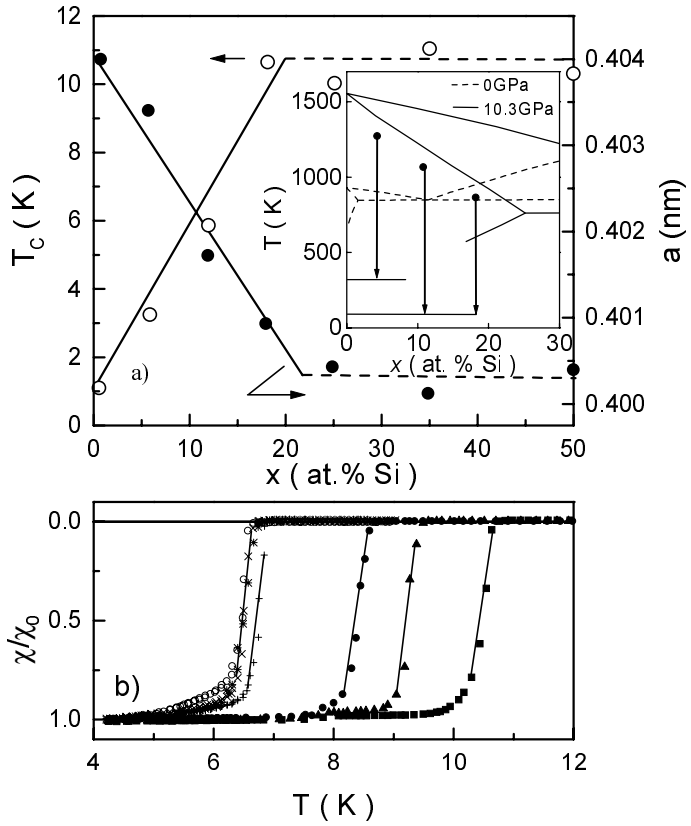

Figure 1. (a) The Si content dependence of the superconducting transition temperature T_c (○) and lattice constant (●) for $Al_{1-x}Si_x$ solid solutions. In the inset: the Al–Si phase diagram for different pressures and the synthesis scheme for $Al_{1-x}Si_x$ solid solutions (arrows). (b) The normalized magnetic susceptibility of the $Al_{1-x}Si_x$ samples with $x > 0.08$ around T_c.

homogeneous substitutional solid solutions $Al_{1-x}Si_x$ with $x \leqslant 0.18$ can be obtained and investigated as model non-equilibrium superconductors well below room temperature. An almost complete diamagnetic response has been found for all samples under investigation; in particular, for $Al_{1-x}Si_x$ solid solutions with high ($x > 0.08$) Si concentrations, the magnetic susceptibility data are presented in figure 1(b). Furthermore, the comprehensive study of magnetotransport [10], Al L_{II-III} x-ray emission spectra together with low-temperature heat capacity [11] and thermoelectric power [12] measurements allow one to distinguish between the different mechanisms of superconductivity enhancement in $Al_{1-x}Si_x$. It was deduced that strong electron–phonon interaction with 'soft cluster modes' is probably the main reason for the dramatic T_c-changes in $Al_{1-x}Si_x$ very close to the FCC lattice instability point.

Among the wide set of experimental data and earlier-studied physical parameters [6–12] there are only preliminary results on ^{27}Al NMR measurements on non-equilibrium $Al_{1-x}Si_x$ solid solutions. At the same time, the NMR technique is a powerful tool for investigating the electronic structure and quasiparticle interactions as well as the features of the local environment of the impurity atoms and characteristics of the short-range order in the disordered metals and compounds. In this work we present the results of ^{27}Al spin–lattice relaxation measurements in combination with the study of quadrupole effects in ^{27}Al NMR spectra for these disordered metallic compounds. Additionally, to introduce direct experimental information about the behaviour of the Eliashberg function $\alpha^2(\omega)F(\omega)$ (where $\alpha(\omega)$ is the electron–phonon interaction function, $F(\omega)$ is the spectral density of phonon states), the point-contact spectra have been studied for $Al_{1-x}Si_x$ at liquid-helium temperatures.

2. Experimental details

The $Al_{1-x}Si_x$ solid-solution samples were prepared by quenching under high pressure (up to 8 GPa) in a toroidal high-pressure chamber. The details of the synthesis procedure and sample characterization have been published elsewhere [9, 10]. Additionally we have studied also a pure Al (99.9%) sample thermally processed at high pressure under conditions similar to those of the high-pressure synthesis. The ^{27}Al NMR experiments were carried out at a magnetic field of 13.8 T in the temperature range 2–300 K using a conventional pulsed Fourier-transform (FT) spectrometer. In the temperature range 130–450 K we also used a commercial Bruker CXP-300 FT spectrometer with a magnetic field 7.01 T. The ^{27}Al NMR spectra were obtained by Fourier transformation of the echo signal after a $\pi/2$–π pulse sequence using a simple four-phase cycling technique. In order to observe the full satellite structure of the powder spectra, which is spread over the frequency range ± 200 kHz around the main ($-1/2 \Leftrightarrow 1/2$) line, we use a short $\pi/2$ pulse of 1.5–2 μs pulse duration. The aluminium nuclear spin–lattice relaxation rate was measured using the saturation–recovery method with variable delay time τ between the saturation train and the spin-echo sequence. To minimize the decrease of the resonance coil quality factor, the samples of $Al_{1-x}Si_x$ ($x = 0$, 0.02, 0.04, 0.06 and 0.08) alloys were prepared as stacks of five or six discs with the diameter of 4 mm and a thickness less than 0.15 mm and glued using dielectric glue. The skin-depth value of pure Al at 150 MHz is $\delta \approx 6.9$ mm [13] which corresponds approximately to 17 000 times the lattice parameter $a(\mathrm{Al}) \approx 4$ Å (see figure 1(a)). This allows us to conclude that the majority of the ^{27}Al NMR signal originated from the bulk of the sample and is not a surface effect. The samples were placed in the coil with the surface of the discs parallel to the coil axis. The superconducting transition temperatures for the $Al_{1-x}Si_x$ samples were determined using dc magnetization measurements. The current–voltage characteristics of the metallic point contacts were investigated by the standard low-frequency modulation technique [14]; the second-harmonic measurements were carried out at temperatures of 1.8–4.2 K. The mechanical $Al_{1-x}Si_x$–$Al_{1-x}Si_x$ point contacts were produced

by causing the samples of the solid solutions to touch in the needle-anvil configuration at liquid-helium temperature.

3. Results and discussion

The ^{27}Al spectra for $Al_{1-x}Si_x$ solid solutions of different contents and for the sample $Al_{0.92}Si_{0.08}$ measured at different values of τ are presented in figure 2 and figure 3 respectively. As a reference, high-quality Al metal film (99.999% purity, Good Fellow Cambridge Limited) has been used. No measurable temperature dependence of the ^{27}Al central-line Knight shift has been observed for any $Al_{1-x}Si_x$ samples. The Knight shift dependence on the silicon concentration x is shown in the inset in figure 2. In the region $0 \leqslant x < 0.1$ the Knight shift is revealed to be a gradually decreasing linear function of the Si content x with the rate $dK/dx = -0.075$. Using the relationship

$$K = \frac{a\chi_s}{g\mu_B\gamma_I h} \sim aN(E_F) \tag{1}$$

(a is the hyperfine interaction constant, χ_s is the electron spin susceptibility, γ_I is the nuclear gyromagnetic ratio, μ_B is the Bohr magneton and $N(E_F)$ is the electronic density of states at the Fermi energy), the variation of the Knight shift (see the inset in figure 2) can be attributed

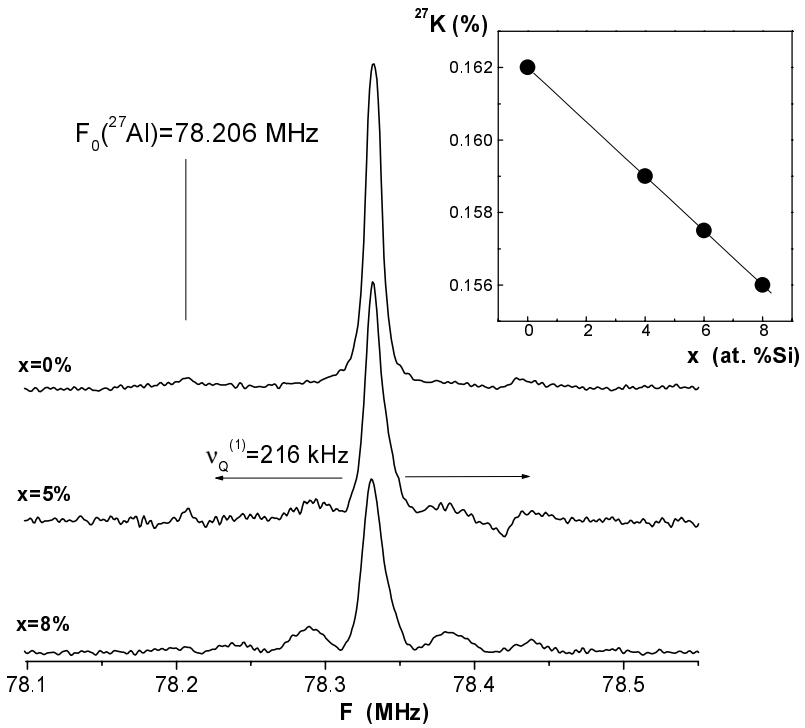

Figure 2. ^{27}Al NMR spectra of $Al_{1-x}Si_x$ alloys with different Si contents x measured at 300 K in a magnetic field of 7 T. The upper spectrum corresponds to the Al sample without Si which was treated by the same thermal-pressure procedure as had been used for all other samples studied. The position of the resonance frequency F_0 of the bare ^{27}Al nuclei is indicated by the vertical line. The inset shows the ^{27}Al Knight shift as a function of the Si content x. The solid line is the linear regression with $dK/dx = -0.075$.

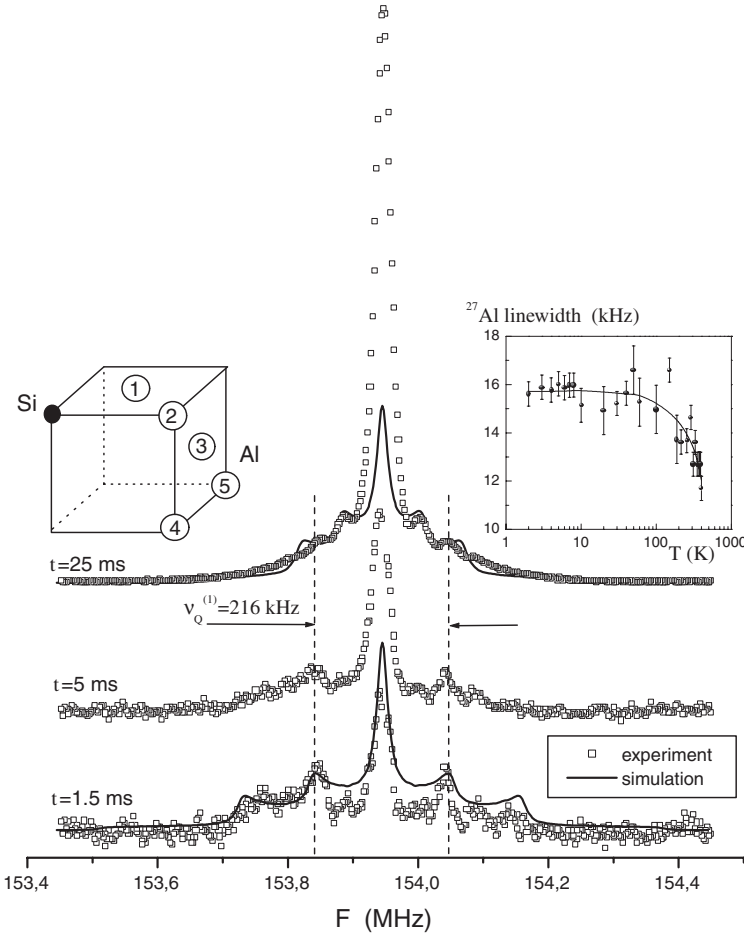

Figure 3. ^{27}Al NMR spectra of $Al_{0.92}Si_{0.08}$ measured at different τ. In the insets: the ^{27}Al linewidth (right panel) is shown as a function of temperature; the local environment of a Si impurity atom (left panel) is presented schematically.

to the decrease of the hyperfine interaction constant, which is determined by the magnitude of the electron wave function near the Al nucleus. Indeed, the investigation of Al L_{II-III} x-ray emission spectra of $Al_{1-x}Si_x$ ($x = 0$–0.1) [11] has not indicated any changes of the 'bare' $N(E_F)$ parameter, while the renormalized electronic density of states $N^*(E_F) = N(E_F)(1+\lambda)$ as deduced from low-temperature heat capacity measurements (λ is the dimensionless electron–phonon interaction constant) was found to increase gradually with elevation of the Si content in $Al_{1-x}Si_x$ solid solutions (up to $\lambda \approx 0.9$ in $Al_{0.92}Si_{0.08}$ [11]). Thus, the decline of $K(x)$ for ^{27}Al NMR spectra (see the inset in figure 2) can be attributed to the noticeable decrease of the electronic charge density in the vicinity of the Al nuclei (i.e., the progressive transfer of s-electron density from Al to Si atoms as the substitution takes place). It is worth emphasizing that the information available from Knight shift measurements is restricted to the s-electron contribution to the density of states at the Fermi surface. Therefore it is necessary to take into account the quadrupolar effects which are related to the total screening charge density at different distances from the impurity. These effects are generally much more important,

although very complicated for supersaturated $Al_{1-x}Si_x$ solid solutions, resulting both from high impurity concentration (up to 0.08 of Si in the study) and the non-equilibrium Si state of these alloys.

Typical first-order quadrupole structure for the spin-$I = 5/2$ ^{27}Al NMR is clearly seen in the spectra presented in figure 2 and figure 3 for the $Al_{0.92}Si_{0.08}$ sample. A powder pattern simulation was performed for these spectra, measured at $\tau = 1.5$ ms and $\tau = 25$ ms. At the low τ-value of 1.5 ms, the simulated pattern corresponds to the quadrupolar frequency $\nu_Q \approx 216$ kHz. The value of ν_Q can be also determined directly from the powder spectrum as a frequency distance between the inner satellite lines (see figure 3). These lines correspond to the singularities of the powder pattern of $(\pm 1/2) \Leftrightarrow (\pm 3/2)$ transitions. Exactly the same quadrupole frequency ν_Q of 217 kHz was observed earlier by Minier and Ho Dung [15] for Al–Si with $x = 0.0004$ of Si and by Stiles and Williams [16] with $x = 0.0025$. This frequency has been attributed in [15, 16] to the Al sites nearest to the Si atom. It is worth mentioning that traces of the same quadrupole structure are observed also for the pure Al sample (see figure 2, upper spectrum) which has been thermally processed at high pressure similarly to other $Al_{1-x}Si_x$ samples. However, the pronounced quadrupole components in the ^{27}Al NMR spectra (figure 2 and figure 3) are certainly caused by the effects of Si-for-Al substitution in the non-equilibrium Al-based matrix.

On increasing the delay time τ up to 5 ms, the quadrupole satellite structure of the ^{27}Al NMR spectrum becomes less clear (see figure 3). At τ-values of about 25 ms a distinct satellite pattern can be observed again with an acceptable signal-to-noise ratio (the top spectrum in figure 3). In contrast with the results at $\tau = 1.5$ ms, this spectrum exhibits additional inner satellites with unusual frequencies $\nu_Q \approx 114$ kHz (see also figure 2; the $x = 0.08$ spectrum recorded at 300 K) while the singularities at 216 kHz are still observable (marked by vertical dashed lines in figure 3). It should be noted that in this case the simulation procedure has been optimized to give the best fit to the inner (the strongest) satellites.

Another interesting feature was revealed while comparing the spectra at $\tau = 1.5$ ms and $\tau = 25$ ms. At low τ-values the relative intensities of the central peak which corresponds to the $(-1/2) \Leftrightarrow (1/2)$ transition and the satellite lines satisfactorily coincides with the simulated powder spectrum. In contrast, the observed intensity of the central peak recorded at the delay time $\tau = 25$ ms is about three times higher than that in the simulated spectrum with the same intensity of the satellite structure.

In order to explain the observed phenomena, we assumed that at low τ, i.e. just after the saturation pulse, one can observe only the fast-relaxing spectral component which is characterized by the shortest spin–lattice relaxation time T_1. In accordance with [15, 16] it is natural to refer this fast component with $\nu_Q \approx 216$ kHz to the Al nuclei which are the nearest neighbours to the Si atoms in the Al-based FCC lattice. These nearest neighbours of the impurity are placed in the [110] direction from Si (site 1 in the left inset in figure 3). The ^{27}Al nuclei from the next atomic shells have the longer relaxation time T_1 and do not contribute to the spectrum at low τ. On increasing the delay time τ, the second-, third- and fourth-neighbour Al atoms (marked 2, 3 and 4 in the left inset in figure 3, respectively) are included in the formation of the spectral intensity. However, the contributions from the $(1/2) \Leftrightarrow (3/2)$ and $(3/2) \Leftrightarrow (5/2)$ transitions of these shells show quadrupole splitting which is less than that for the first neighbour and is comparable to the linewidth ($\nu_Q^{(2)} < 15$ kHz [15], $\nu_Q^{(3)} \approx 44$ kHz [15, 16] and $\nu_Q^{(4)} \approx 19$ kHz [15] or $\nu_Q^{(4)} \approx 37$ kHz [16]), so one can expect a substantial enhancement of the central-peak relative intensity and the appearance of a noticeable dip around the main line. Since for the dilute Al–Si alloys the quadrupole frequency value $\nu_Q^{(2)}$ is much less than $\nu_Q^{(3)}$, the inner satellites observed at $\tau = 25$ ms can be attributed to the $(1/2) \Leftrightarrow (3/2)$ transition of the 3d nearest neighbours.

Additionally, taking into account a strong distortion of the FCC Al-based structure (Al- and Si-atom displacements from their sites) which takes place in the vicinity of the lattice instability in these supersaturated $Al_{1-x}Si_x$ solid solutions, it is natural to expect an effective mixing of these next-nearest-neighbour quadrupole contributions to the dip (or the 'wings' of the resonance signal [18]). Moreover, the situation happens to be much more complicated and difficult to analyse quantitatively because of the high impurity (Si atoms) concentration in these alloys and, as a result, very strong superposition of electric field gradients from different Si atoms at Al sites. Also, it is possible to find an analogy between these non-equilibrium crystalline materials and metallic glasses for which large local atomic displacements and the softening of the phonon modes are believed to be important [19].

To clarify the role of the disordering and non-equilibrium effects in the formation of the above-mentioned features of ^{27}Al NMR spectra, additional measurements of the resonance linewidth have been carried out at temperatures of 2–450 K. It was certainly established (see the right inset in figure 3) that for temperatures above 200 K the central resonance line starts to narrow. The 'narrowing temperature' $T_n \approx 200$ K defined here for non-equilibrium $Al_{1-x}Si_x$ alloy with $x = 0.08$ is much smaller than $T_n \approx 340 \pm 10$ °C determined for the case of Al self-diffusion in pure Al [20] and in Al–Zn alloys [17]. Therefore one can conclude that the non-equilibrium effects in these $Al_{1-x}Si_x$ supersaturated solid solutions have appreciable importance. Additional arguments in favour of this kind of interpretation have been provided very recently by the study of the decay kinetics of non-equilibrium $Al_{1-x}Si_x$ solid solutions [9]. A small activation energy value $E_a \approx 80$ kJ mol^{-1} for Si-atom diffusion in the supersaturated Al-rich matrix of $Al_{1-x}Si_x$ with $x < 0.2$ was determined. This compares with $E_a \approx 130$ kJ mol^{-1} for isolated Si atoms and can be interpreted in terms of a strong reduction of the barriers for Si-atom diffusion in Al. The strong lattice distortion of the non-equilibrium FCC matrix has been deduced from resistivity relaxation data and scanning calorimetry measurements [9], in support of the significant screening asymmetry behaviour for high Si contents.

From this point of view, appreciable changes of the electric field gradients (EFG) and asymmetry parameter η with the silicon concentration x in the non-equilibrium Al-based matrix may be considered as the main reason for the discrepancy between $\nu_Q \approx 44$ kHz found in [15, 16] for dilute Al–Si alloys and $\nu_Q^{(3)} \approx 114$ kHz observed in the present work for the $Al_{0.92}Si_{0.08}$ sample (see, for example, figure 3, upper spectrum). Indeed, at low Si content x, one can consider the Si atom in an Al host as an isolated impurity which creates an axially symmetric field gradient $q(r)$ with $\eta = 0.03$–0.06 [15, 16] at the neighbouring Al sites. At high Si contents $x = 0.08$, one can expect the appearance of other Si atoms in the shells nearest to the Al site in the Al-based FCC lattice, resulting in strong enhancement of the EFG and asymmetry of the screening charge density, and causing the increase of $\nu_Q^{(3)}$ in comparison with that for the dilute case.

In the framework of the approach, it is natural to expect the appearance of fast and slow components in the ^{27}Al NMR spin–lattice relaxation process. To study the relaxation in $Al_{0.92}Si_{0.08}$ alloy, magnetization–recovery curves have been recorded for the central-peak intensity as a function of τ. The results obtained at different temperatures are shown in figure 4 in comparison with those for pure Al foil. These dependencies exhibit a distinct double-exponential behaviour and have been fitted with the expression

$$I = I_0 + A_{slow}(1 - \exp(-\tau/T_{1,slow})) + A_{fast}(1 - \exp(-\tau/T_{1,fast})) \qquad (2)$$

where A_{slow} and A_{fast} are the amplitudes of the slow- and fast-relaxing components, respectively. From the data of figure 4 it is easy to see that the fast and slow contributions to the central-line intensity change dramatically between single-fast-exponent relaxation at room

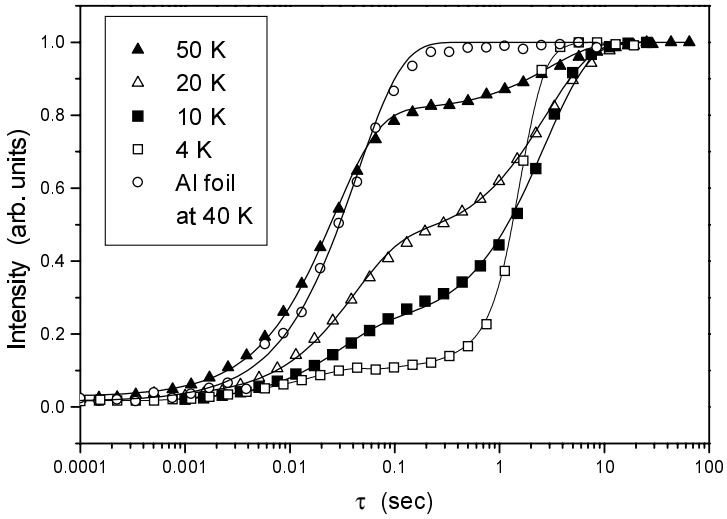

Figure 4. ^{27}Al magnetization–recovery curves for $Al_{0.92}Si_{0.08}$ measured at different temperatures. Solid lines are fits to (2) (see the text).

temperature and behaviour described almost by a single slow exponential at liquid-helium temperature. As a result the ratio, A_{slow}/A_{fast}, drastically decreases with temperature by a factor of about 100 (see figure 5(a)). Moreover, the slow component of the spin–lattice

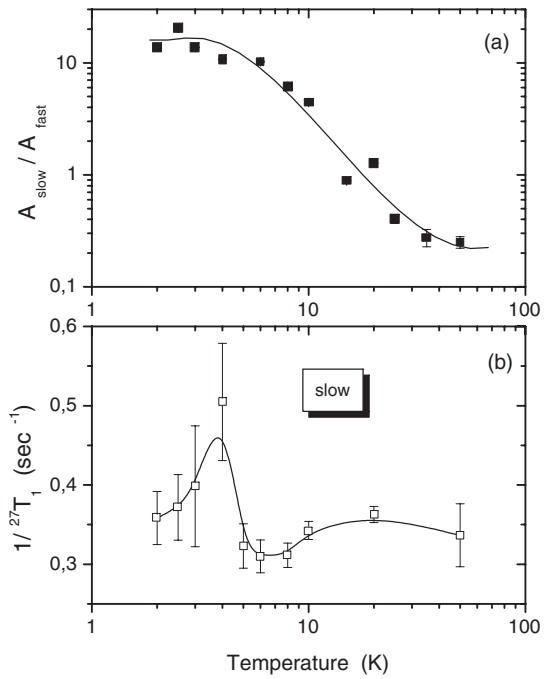

Figure 5. Temperature dependencies of (a) the ratio $A_{\rm slow}/A_{\rm fast}$ (see the text) and (b) the spin–lattice slow-relaxation component for $Al_{0.92}Si_{0.08}$.

relaxation completely disappears at temperatures above 60 K, and therefore it is possible to exclude the possibility of a trivial interpretation of the double-exponential behaviour as a superposition of two macroscopic phases in the $Al_{1-x}Si_x$ sample. Indeed, in the case where Si-enriched and pure Al phases exist in the alloy, the ratio should be independent of temperature, in contrast with the results of figure 5(a).

The resulting temperature dependencies of the slow- and fast-relaxation components are presented in figure 5(b) and figure 6(b), respectively. For comparison, in figure 6(b) we also plot the experimental $1/T_1$ values measured for the pure Al foils, which are perfectly described by the Korringa relationship: $T_1T = 1.85$ s K [21]. As seen from this figure, $1/T_{1,\mathrm{fast}}$ follows the Korringa law at high temperatures of 100–450 K but deviates from the linear $1/T_1$ dependence below 100 K. The above-mentioned substantial increase of the $1/T_1$ parameter at low temperatures both in fast- and slow-relaxation channels (figure 5(b), figure 6(b)) may be attributed to the strong renormalization of the electronic density of states $N^*(E_F)$ in the non-equilibrium $Al_{1-x}Si_x$ solid solutions. Using a Korringa expression [22]:

$$1/(T_1TK^2) = \frac{4\pi k_B}{\hbar}\left(\frac{\gamma_1}{\gamma_e}\frac{\chi_0}{\chi_s}\frac{N^*(E_F)}{N(E_F)}\right)^2 \tag{3}$$

(γ_e is electron gyromagnetic ratio, χ_s and χ_0 are the spin susceptibility of collective and free electrons respectively, k_B is the Boltzmann constant) and taking into account the enhancement

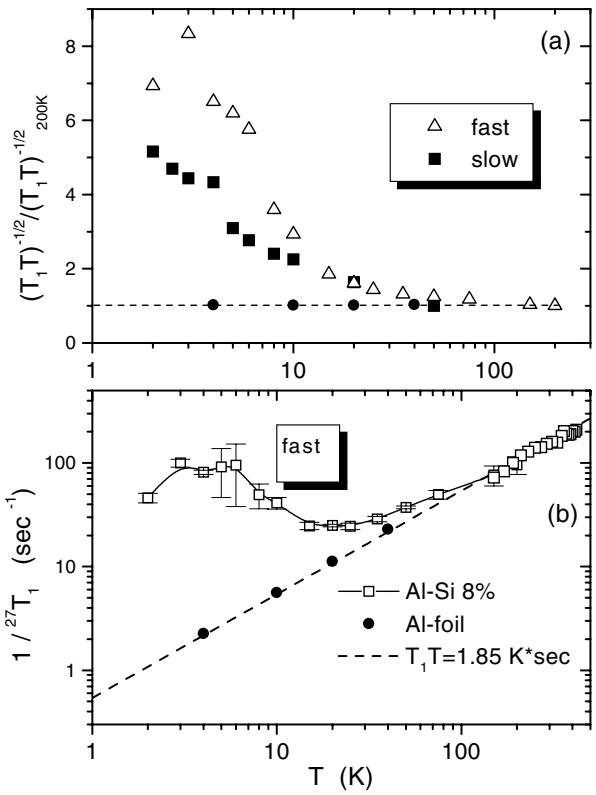

Figure 6. (a) A temperature plot of the product $(T_1T)^{-1/2}$ normalized on its value at 200 K. (b) The spin–lattice fast-relaxation component in $Al_{0.92}Si_{0.08}$ as a function of temperature. Solid lines are just guides for the eye. The dashed line in (b) corresponds to the Korringa ratio $T_1T = 1.85$ s K for pure Al [17]. Solid circles in (b) show the experimental values for pure Al foil.

of quasiparticle interactions in these model superconductors [12], it is possible to estimate the changes in $N^*(E_F)$ from the data of figure 5(b) and figure 6(b). An additional assumption that $\chi_s(T) =$ constant may be used for these wide-band metals (for $Al_{1-x}Si_x$, the bandwidth is found to be 11 eV [11]). This approach allows one to attribute the dramatic changes of the normalized $(TT_1)^{-1/2}$ parameter (figure 6(a)) directly to variation of the density of states $N(E_F)$. Moreover, an argument in favour of this kind of interpretation can be obtained from well-known discussions (see, for example, [23]) concerning the role of renormalization effects in various physical parameters. In particular, there is no contribution from the electron–phonon interaction mechanism predicted for spin susceptibility in metals, so it is natural to consider the observed increase of $(TT_1)^{-1/2}$ (figure 6(a)) as a feature of $N^*(E_F)$ transformation with temperature in these non-equilibrium $Al_{1-x}Si_x$ superconductors. At the same time, the extracted enhancement factor $1 + \lambda \approx 4$–7 (figure 6(a)) seems to be far above its value of ∼1.5 determined from the heat capacity measurements [11] on the $Al_{0.92}Si_{0.08}$ sample. A possible explanation of the discrepancy is a substantial variation of the electron–phonon coupling with different vibrations and, as a result, a strong dispersion of the NMR-deduced enhancement factor $1 + \lambda$ between different relaxation channels (figure 6(a)). It is interesting to note here the results of dynamical property calculations obtained for $Al_{0.99}Si_{0.01}$ solid solution in [24], where much more pronounced softening was revealed along [110] and [100] than in other directions from the Si impurity (see the left inset in figure 3). However, in this way we have to conclude that the data from ^{27}Al spin–lattice relaxation measurements (figure 4–figure 6) cannot be quantitatively described in terms of the Korringa approach, so the problem of an analysis and adequate interpretation of the results discussed remains open.

To shed more light on the origin of these phenomena in the model superconductors, one needs to characterize in more detail the electron–phonon interaction in $Al_{1-x}Si_x$ non-equilibrium solid solutions. Although the phonon density of states $F(\omega)$ changes only slightly under Si-for-Al substitution [25], T_c increases dramatically in $Al_{1-x}Si_x$ and the appearance of the low-temperature anomalies in the transport and Seebeck coefficients has been interpreted [10–12] in terms of a strong renormalization of the Eliashberg function $G(\omega) = \alpha^2(\omega)F(\omega)$ at low frequencies.

To obtain additional and direct evidence of the enhancement of the electron–phonon interaction $\alpha^2(\omega)$ for $Al_{1-x}Si_x$, a study of point-contact (pc) spectra has been carried out in the present work. The measured d^2I/dU^2 curves are shown in figure 7. The data for pure Al (curve 1 in figure 7) are presented as a reference and reproduce well-known results [26]: two peaks at 21 and 36 meV correspond to electron–phonon interaction with LA and TA modes respectively. However, in the case of the non-equilibrium substitutional solid solutions $Al_{1-x}Si_x$ with high Si content, a transition from the ballistic to the thermal regime of the point contact takes place. As a result, the phonon features of the point-contact spectra decrease by a factor of l_i/d (where d is the contact diameter and l_i is the mean free path of the charge carriers) and hence only the range of small Si concentrations is appropriate for qualitative analysis of the pc Eliashberg function behaviour. In the point-contact spectra of $Al_{1-x}Si_x$ with $x > 0.02$, the LA and TA features are suppressed gradually, in contrast with the onset and increase of magnitude of the low-frequency anomaly in d^2I/dU^2 characteristics (curves 3, 4 in figure 7). Thus, the noticeable increase of the pc Eliashberg function $G_{pc}(\omega) \sim d^2I/dU^2$ which is observed in the frequency range $\hbar\omega < 15$ meV (figure 7) can be attributed to the effects of an enhancement of the electron–phonon interaction $\alpha^2(\omega)$ under Si-for-Al substitution. As a result of the enhancement, a density-of-states renormalization $N^*(E_F)$ and a gradual T_c increase already take place for small enough Si contents in non-equilibrium $Al_{1-x}Si_x$ solid solutions.

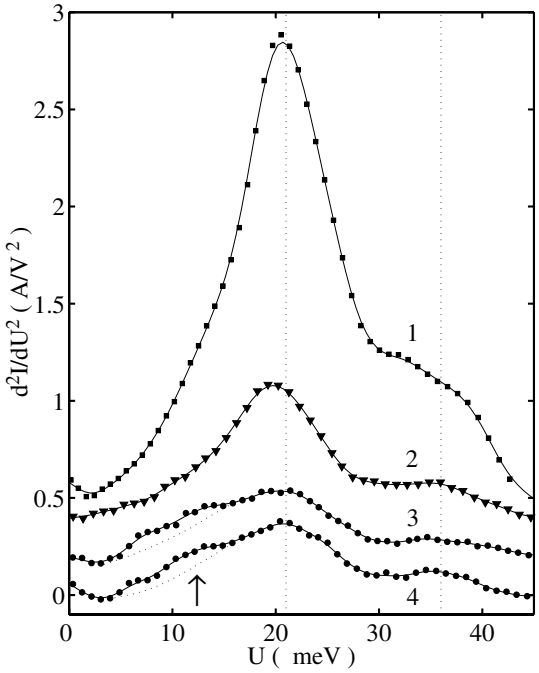

Figure 7. Point-contact spectra of pure Al (curve 1) and solid solutions $Al_{1-x}Si_x$: $x = 0.015$ (curve 2) and 0.025 (curves 3, 4) at $T = 1.8$ K.

4. Conclusions

In conclusion, we have used ^{27}Al NMR and point-contact spectroscopy techniques to investigate the normal-state parameters and electronic structure of the non-equilibrium $Al_{1-x}Si_x$ solid solutions. When the temperature decreases between 300 K and 2 K, a dramatic transformation of the ^{27}Al NMR behaviour occurs in $Al_{0.92}Si_{0.08}$: the deviation from the Korringa-type behaviour below 100 K is accompanied by the appearance of a double-exponential relaxation process at intermediate temperatures. Moreover, both the fast- and slow-relaxation rates exhibit a pronounced maximum at liquid-helium temperature. A substantial change of the quadrupole component in the ^{27}Al NMR spectra has been found for concentrated $Al_{1-x}Si_x$ ($x > 0.02$) solid solutions in comparison with that for low-Si-content alloys ($x \leqslant 0.025$). The results of ^{27}Al NMR linewidth measurements also confirm the existence of strong distortion and disordering effects of the Al-based structure in the vicinity of the lattice instability in these non-equilibrium $Al_{1-x}Si_x$ metals. It was shown that a variety of the new experimental results can be interpreted in terms of an enhancement of the electron–phonon interaction and, as a result, a strong renormalization of the electronic density of states $N^*(E_F)$ in these model superconductors.

Acknowledgments

The authors wish to express their gratitude to Professor K Luders for fruitful discussions and O Klein and W Hoffmann for assistance with the ^{27}Al NMR measurements. This work was supported by INTAS programme 96-451, the Russian Foundation for Basic Research Grants N17163 and N16067, the programmes ‘Fundamental Spectroscopy’ and ‘Microwaves’ of the Russian Ministry of Science and Technology and the Copernicus Network ERB IC15 CT98 0812.

References

[1] Douglass N V and Meservey R Jr 1964 *Phys. Rev.* A **19** 135
[2] Lamoise A M, Chaumont J, Meunier F and Bernas H 1975 *J. Physique Lett.* **36** 271
[3] Lamoise A M, Chaumont J, Lalu F, Meunier F and Bernas H 1976 *J. Physique Lett.* **37** L287
[4] Tsuei C and Johnson W L 1974 *Phys. Rev.* B **9** 4742
[5] Mii H, Senoo M and Fujishiro I 1976 *Japan. J. Appl. Phys.* **15** 777
[6] Degtyareva V F, Chipenko G V, Belash I T, Barkalov O I and Ponyatovskii E G 1985 *Phys. Status Solidi* a **89** K127
[7] Sluchanko N E, Glushkov V V, Demishev S V, Samarin N A, Savchenko A K and Brazhkin V V 1994 *J. Phys.: Condens. Matter* **6** 9079
[8] Sluchanko N E, Glushkov V V, Demishev S V, Samarin N A and Brazhkin V V 1996 *Phys. Rev.* B **53** 11 304
[9] Sluchanko N E, Glushkov V V, Demishev S V, Kondrin M V, Ischenko T V, Gust W, Brazhkin V V, Straumal B B, Bruynseraede Y and Moshchalkov V V 2000 *Phys. Rev.* B **61** 6019
[10] Brazhkin V V, Glushkov V V, Demishev S V, Kosichkin Yu V, Sluchanko N E and Shulgin A I 1993 *J. Phys.: Condens. Matter* **5** 5933
[11] Sluchanko N E, Glushkov V V, Demishev S V, Samarin N A, Savchenko A K, Singleton J, Hayes W, Brazhkin V V, Gippius A A and Shulgin A I 1995 *Phys. Rev.* B **51** 1112
[12] Sluchanko N E, Glushkov V V, Demishev S V, Kondrin M V, Samarin N A, Savchenko A K, Orlov A O, Snider G L, Brazhkin V V and Moshchalkov V V 1997 *Phys. Rev.* B **56** 10 816
[13] *Bruker Almanac* 1998 (Karlsruhe: Bruker GmbH)
[14] Jansen A G M, van Gelder A P and Wider P 1980 *J. Phys. C: Solid State Phys.* **13** 6073
[15] Minier M and Ho Dung S 1977 *J. Phys. F: Met. Phys.* **7** 503
[16] Stiles J A R and Williams D Ll 1974 *J. Phys. F: Met. Phys.* **4** 2297
[17] Webb M B 1961 *J. Phys. Chem. Solids* **20** 127
[18] Gruner G and Minier M 1977 *Adv. Phys.* **26** 231
[19] Beck H and Guntherodt H J (ed) 1983 *Glassy Metals II (Springer Topics in Applied Physics vol 53)* (Berlin: Springer)
[20] Spokas J J and Slichter C P 1959 *Phys. Rev.* **113** 1462
[21] Carter G C, Bennett L H and Kahan D J 1974 *Metallic Shifts in NMR* part 1 (Oxford: Pergamon)
[22] Abragam A 1961 *The Principles of Nuclear Magnetism* (Oxford: Clarendon)
[23] Opsal J L, Thaler B J and Bass J 1976 *Phys. Rev. Lett.* **36** 1211
[24] Caro A, Drabold D A and Sankey O F 1994 *Phys. Rev.* B **49** 6647
[25] Chevrier J, Suck J B, Lasjaunias J C, Perroux M and Capponi J J 1994 *Phys. Rev.* B **49** 961
[26] Pepper M 1980 *J. Phys. C: Solid State Phys.* **13** L717